



Article

IL-Functionalized Mg₃Al-LDH as New Efficient Adsorbent for Pd Recovery from Aqueous Solutions

Laura Cochechi , Lavinia Lupa * , Nick Samuel Tolea, Radu Lazău and Rodica Pode *

Faculty of Industrial Chemistry and Environmental Engineering, Politehnica University Timisoara,
Blv. Vasile Parvan No. 6, 300223 Timisoara, Romania

* Correspondence: lavinia.lupa@upt.ro (L.L.); rodica.pode@upt.ro (R.P.)

Abstract: Palladium is a noble metal of the platinum group metals (PGMs) with a high value and major industrial applications. Due to the scarce palladium resources, researchers' attention is currently focused on Pd ions recovery from secondary sources. Regarding the recovery process from aqueous solutions, many methods were studied, amongst which adsorption process gained a special attention due to its clear advantages. Moreover, the efficiency and the selectivity of an adsorbent material can be further improved by functionalization of various solid supports. In this context, the present work aims at the synthesis and characterization of Mg₃Al-LDH and its functionalization with ionic liquid (IL) (Methyltrialkylammonium chloride) to obtain adsorbent materials with high efficiency in Pd removal from aqueous solutions. The maximum adsorption capacity developed by Mg₃Al-LDH is 142.9 mg Pd., and depending on the functionalization method used (sonication and co-synthesis, respectively) the maximum adsorption capacity increases considerably, q_{\max} -Mg₃Al IL-US = 227.3 mg/g and q_{\max} -Mg₃Al IL-COS = 277.8 mg/g.

Keywords: adsorption; double layered hydroxides; ionic liquids; palladium



Citation: Cochechi, L.; Lupa, L.; Tolea, N.S.; Lazău, R.; Pode, R.

IL-Functionalized Mg₃Al-LDH as New Efficient Adsorbent for Pd Recovery from Aqueous Solutions. *Int. J. Mol. Sci.* **2022**, *23*, 9107. <https://doi.org/10.3390/ijms23169107>

Academic Editor: Jun Wang

Received: 1 July 2022

Accepted: 11 August 2022

Published: 14 August 2022

Publisher's Note: MDPI stays neutral with regard to jurisdictional claims in published maps and institutional affiliations.



Copyright: © 2022 by the authors. Licensee MDPI, Basel, Switzerland. This article is an open access article distributed under the terms and conditions of the Creative Commons Attribution (CC BY) license (<https://creativecommons.org/licenses/by/4.0/>).

1. Introduction

Palladium (Pd) is part of the platinum group metals (PGMs), which were identified by the European Commission as part of the 27 “critical” raw materials with economic importance [1]. Its chemical stability and good conducting properties represent the most important reasons why Pd is used in so many important fields, such as: electronic and telecommunication industries, catalytic applications, medicine, etc. Due to its intensive use in the last years, it could be found in higher concentrations in secondary sources compared with the concentrations from natural ores [2]. Thus, special attention was paid to reclaiming Pd from secondary sources, especially from wastewaters. One of the most efficient methods of Pd recovery from aqueous solutions is adsorption, due to its numerous advantages: high performance, ease of operation, low-cost, wide operability [3–5]. Wojnicki et al. recovered palladium (II) chloride complex ion by adsorption onto charcoal (maximum adsorption capacity $q_m = 42.4$ mg/g at 323 K) [6], Zhang et al. studied nanosilica modified with imidazolium, groups as adsorbent material for Pd recovery from aqueous solutions ($q_m = 69.6$ mg/g) [2], Chitosan and modified chitosan were also used as adsorbent materials [7,8]. The list of examples can go on, but the interest in finding the most effective adsorbent for recovering Pd ions from aqueous solutions is still relevant. The challenge in the adsorption processes is to use an adsorbent material with the following key features: high adsorption capacity, high output/efficiency, easy to synthesize, stable and reusable. All these characteristics are associated with layered double hydroxide materials. Layered double hydroxide materials (LDH) are lamellar structure solids, also known as anionic clays, which can be synthetically prepared in a great number of possible composition and metal anions combinations. Unique and ordered structure, flexible tunability, high chemical and thermal stability, ability to intercalate different type of anions, are just a few properties, which make LDH superior to other adsorbent materials [9,10].

In the last decade, to enhance the adsorption properties of LDH materials, the researchers focused on their structure functionalization/modification with different pendant or functional groups. Tang et al. published a comprehensive review regarding the functionalization of LDH materials, through (i) intercalation of different molecules, (ii) surface modification, (iii) LDH loading on different substrates by in situ growth, which were used for the adsorption of various metal ions (Ag^+ , Pb^+ , Cu^{2+} , Cd^{2+} , Co^{2+} , Zn^{2+} , Ni^{2+}) from aqueous solutions [11]. Another review about functionalized LDH used for anionic and cationic removal from aqueous solutions was published by Ishak et al. [12]. In conclusion, functionalized LDHs have better selective absorption capacity, stability, and recyclability. Ionic liquids are salts, in the liquid state at room temperature, which contain both an anion and a cation. Due to their useful physico-chemical properties, such as high thermal and chemical stability, low volatility, and very high ability to dissolve a wide range of compounds, they gained a particular attention for application as functional element for the structural modification of different materials. It was observed that by using ionic liquids, functionalized materials were obtained with superior adsorbent behavior in many applications: CO_2 separation [13,14], dyes removal [15,16], metal ions adsorption [17,18]. ILs were also used for LDH functionalization/modification to obtain materials with superior catalytic performance [19–21], or improved anionic exchange membranes [22]. From our knowledge, there are no published data to discuss the functionalization of Mg_3Al -LDHs with ionic liquids to be used as adsorbent materials for the removal of metal ions from aqueous solutions. In our recently published paper [23], we studied the sequential use of ionic liquid-functionalized Zn-Al layered double hydroxide as adsorbent and photocatalyst, which presented very good performance in both of the studied water treatment techniques. However, in a review published recently by Tang et al., the important role of HO^- group and valence state of $[\text{Mg}(\text{OH})_6]$ octahedron in the synthesis of functionalized layered double hydroxides using various method (intercalation, surface loading or modification) is underlined [11]. Therefore, the purpose of this paper was the obtaining and characterisation of a new efficient adsorbent material for palladium recover from aqueous solutions. The new adsorbent material consists from Mg_3Al -LDH which was functionalized with Methyltrialkylammonium chloride ionic liquid. The functionalization of Mg_3Al -LDH with the studied ionic liquid was carried by two methods: ultrasonic method and co-synthesis. The used ionic liquid was Methyltrialkylammonium chloride, based on the reports of its effect in improved adsorption properties of other impregnated solid supports, such as chitosan, Zn_3Al , or alginate, used for removal of lead ions, dyes or phenol from aqueous solutions [24–27]. The paper aims the determination of the efficiency of the new synthesized adsorbents materials, the influence of the ionic liquids and the influence of the synthesis method upon the adsorption capacity developed by the synthesized materials in the recovery process of palladium ions from aqueous solutions.

2. Results and Discussion

2.1. Adsorbent Materials Characterization

The X-ray diffraction patterns (Figure 1) were recorded to confirm the phase composition of the synthesized Mg_3Al layered double hydroxides and to observe the IL functionalization effect upon samples structure and crystallinity. The XRD pattern of the Mg_3Al sample showed characteristic peaks of hydrotalcite (JCPDS-41-1428) formed from symmetric, intensive and sharp peaks at low 2θ angle (11.2° and 22.6° and 34.4°), respectively from asymmetric and broad peaks at high 2θ angle (60.3° and 61.5°), suggesting a good sample crystallization. These results are similar with other reported data in literature [28–30].

The calculated lattice parameter, c , offers information about the interlayer distance of the LDH. The values presented in Table 1 clearly show the CO_3^{2-} intercalation in the Mg_3Al IL-US ($c = 23.52 \text{ \AA}$), as compared to Mg_3Al sample ($c = 23.58 \text{ \AA}$) [31].

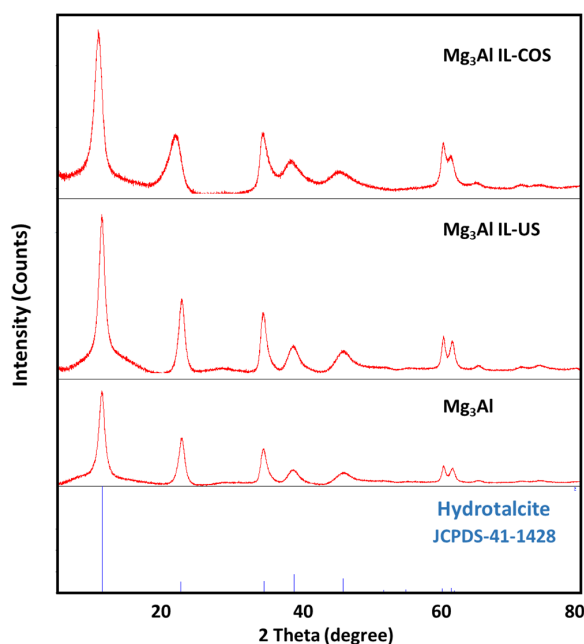


Figure 1. XRD patterns of the studied adsorbent materials.

Table 1. Unit cell parameters and textural properties of the synthesized samples.

Method of Synthesis	Sample Acronym	a (Å)	c (Å)	$d_{(003)}$ (Å)	D (nm)	S_{BET} (m ² /g)	V_p (cm ³ /g)
MgAl-layered double hydroxide synthesized through co-precipitation Mg:Al = 3:1	Mg ₃ Al	3.073	23.58	7.86	4.86	102	0.628
Mg ₃ Al-LDH + IL functionalized by ultrasound method	Mg ₃ Al IL-US	3.071	23.52	7.84	4.45	93.9	0.560
Mg ₃ Al-LDH + IL functionalized by co-synthesis	Mg ₃ Al IL-COS	3.072	24.39	8.13	3.38	22.2	0.168

The IL functionalization of Mg₃Al by ultrasound method does not generate a disorder of the LDH structure. In case of Mg₃Al IL-COS could be observed a shift of the main peaks at lower 2θ values (10.7°, 21.9° and 34.3°). The c parameter for Mg₃Al IL-COS is higher, $c = 24.39$ Å suggesting that through functionalization of Mg₃Al by co-synthesis the intercalation of IL between the LDH interlayer took place, which also led to a slight decrease in the crystallite size (Table 1). For all three samples the typical doublet at approximately 60 degrees 2θ could be observed, and the calculated values of a parameters for (110) planes are around 3.07 Å, which is in good agreement with other data presented in the literature for similar materials [32,33]. The fact that in case of Mg₃Al functionalization through ultrasound method the order of the LDH structure is not disturbed, the studied IL is found on the surface of the LDH, while in case of the co-synthesis method, appears a structure disturbance, the IL being between the LDH layers was evidenced by the morphological analysis of the sample published in our previous work [34].

The thermal analysis (Figure 2) shows the behavior of the samples during the thermal treatment up to 1000 °C. For the Mg₃Al sample, the main thermal decomposition processes (dehydration, dehydroxylation and decarbonization) occur in the temperature intervals: 20–300, 300–700 and above 700 °C. Between 20 and 300 °C, the DSC diagram of Mg₃Al sample reveals an unresolved endothermic shoulder at approximately 85 °C, due to the loss of adsorbed water and an endothermic peak at 188 °C which is due to the loss of interlayer water molecules (dehydration) and partial dehydroxylation (some water molecules formed in the recombination of hydroxyl groups from the brucite-like layer could be removed at this temperature) [35]. The mass loss in this temperature interval is 17.6%. Between 300 and 700 °C, a consistent mass loss takes place (28.0%) accompanied by an endothermic

peak at 395 °C caused by the total dehydroxylation and partial decarbonization of the LDH. A broad endothermic peak and another endothermic peak with maxima at about 740 °C and at 905 °C, respectively, are due to the total decarbonization of the material and the formation of mixed metal oxides. The total mass loss due to the decomposition of Mg₃Al sample is 45.7%.

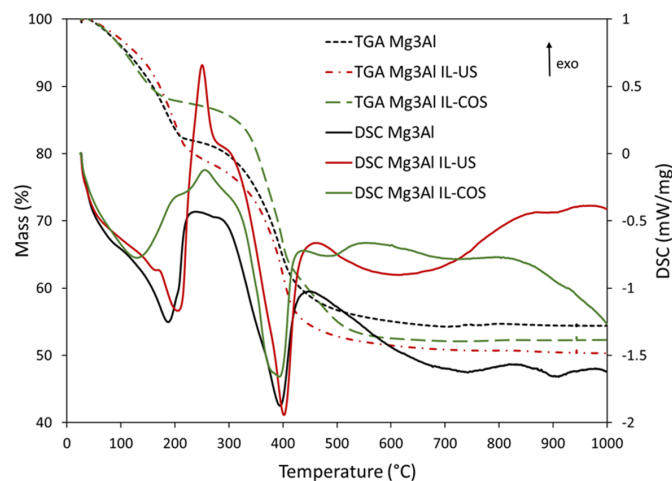


Figure 2. Thermoanalytic curves of the synthesized samples.

By comparison, for the Mg₃Al IL-US sample, the DSC curve reveals the unresolved endothermic shoulder due to the loss of adsorbed water at approximately 70 °C, another endothermic shoulder at 166 °C and an endothermic peak at 206 °C. The presence of two peaks due to the loss of interlayer water molecules and partial dehydroxylation, instead of one, and the displacement (shifting) of the maximum temperature to lower values for the shoulders and at higher value for the peak (as compared to sample Mg₃Al) could be a consequence of the interaction of the organic IL with the physically adsorbed water molecules and those placed in the interlayer space of LDH. The mass loss for this temperature interval is 19.1%, greater than the mass loss of Mg₃Al sample, suggesting that IL interacts also with some hydroxyl anions from the LDH layer, forcing the dehydroxylation process to occur at lower temperature. The sharp exothermic peak with maximum at 251 °C and the unresolved exothermic shoulder at about 300 °C appear due to the combustion of organic chain of ionic liquid. This exothermic peak overlapped to the endothermic peak with maximum at 402 °C, which is due to the dehydroxylation and decarbonization of the LDH. The mass loss for this temperature interval is 30.2%. The broad endothermic peak at approximately 630 °C and the small shoulder at about 900 °C are due to the formation of mixed metal oxides. The total mass loss for Mg₃Al IL-US material is 49.3%.

The appearance of thermoanalytic curves of Mg₃Al IL-COS sample is slightly different from those of the other two samples. Due to the fact that the ionic liquid is placed in the interlayer space, it probably replaced water molecules in this space, and interacted with carbonate anions placed in the interlayer space and with the hydroxyl anions on the brucite-like layer. Thus, in the first temperature range (20–200 °C), the DSC curve shows a single endothermic peak with the maximum at 129 °C, instead of two or three endothermic peaks as the other samples had. Additionally, the mass loss for this temperature range is the lowest (12.5%). The exothermic peak due to the combustion of the ionic liquid shifted to a higher temperature than in the case of the Mg₃Al IL-US sample (256 °C vs. 251 °C), suggesting that a higher energy was needed to break some interactions between IL and LDH. Also, the endothermic peak due to the dehydroxylation and decarbonization of the material is broader, its maximum being observed between 375 and 396 °C, it is followed by an endothermic peak at 480 °C, and the mass loss in this second temperature range (200–700 °C) is the highest, 35.3%. At temperatures higher than 700 °C, an endothermic

shoulder appears due to the formation of mixed, crystalline metal oxides. The total mass loss of this material is 47.9%.

FTIR spectra of the synthesized samples (Figure 3) highlights the presence of carbonate anions and water from the interlayer space, as well as the type of bonds formed in the studied materials. Information can also be obtained on how ionic liquid interacts with layered double hydroxide, depending on the method of materials synthesis (by ultrasonication or co-synthesis).

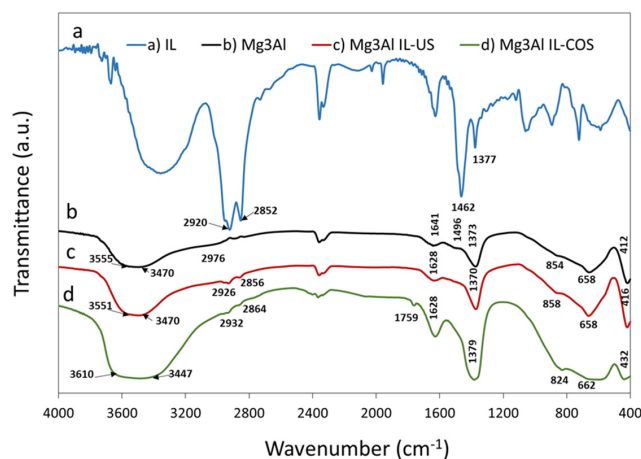


Figure 3. FTIR spectra of the synthesized samples.

The spectrum of ionic liquid Methyltrialkylammonium chloride (Figure 3a) exhibits two absorption bands situated at 2920 cm^{-1} and 2852 cm^{-1} assigned to antisymmetric and symmetric stretching vibration of $-\text{CH}_2-$ and $-\text{CH}_3$ groups, respectively. Usually, the bending vibration of C-H bond of the quaternary ammonium salt with long alkyl chains give two absorption bands near 1460 cm^{-1} specific for C-H bending of both $-\text{CH}_2-$ and $-\text{CH}_3$ groups. The band with the maximum at 1377 cm^{-1} corresponds to the $-\text{CH}_2-$ trans-plane bending vibration [36].

The Mg_3Al FTIR spectrum (Figure 3b) contains the absorption bands that are expected from a layered double hydroxide sample with carbonate as interlayer anion. The broad band at about 3500 cm^{-1} is the result of several bands that are partially overlapping in this region: one band at 3555 cm^{-1} that could be due to the hydroxyl coordinated by both Mg and Al, another band at 3470 cm^{-1} that could be assigned to the Al-OH bond and a shoulder at 2976 cm^{-1} assigned to $\text{CO}_3^{2-}-\text{H}_2\text{O}$ bridging mode of carbonate and water in the interlayer region [37]. The absorption band situated at 1641 cm^{-1} is attributable to the bending mode of water molecules from the interlayer region. The band at 1373 cm^{-1} and the shoulder at 1496 cm^{-1} could be attributed to the ν_3 mode (antisymmetric stretching) of interlayer carbonate anion, the splitting of the band being a sign of the low symmetry of the anion in the interlayer space, probably due to hydrogen bonding with hydroxyl groups or with water molecules [38]. The two bands at 854 cm^{-1} and 658 cm^{-1} are characteristic to the ν_2 and ν_4 vibration modes of carbonate group. The absorption band situated at 412 cm^{-1} is attributable to the vibration mode of the hydrotalcite octahedral network [39].

The spectrum of Mg_3Al IL-US sample (Figure 3c) displays all the bands observed in the Mg_3Al sample. The only noticeable differences between the FTIR spectrum of Mg_3Al and Mg_3Al IL-US sample are: the presence of the absorption bands assigned to $-\text{CH}_2-$ and $-\text{CH}_3$ groups in IL (observed at 2926 cm^{-1} and 2856 cm^{-1}), that overlap with the band assigned to the $\text{CO}_3^{2-}-\text{H}_2\text{O}$ (bridging mode of carbonate and water in the interlayer region), and the shift of the band attributed to the bending mode of water molecules from 1641 cm^{-1} (observed in the spectrum of Mg_3Al sample) to 1628 cm^{-1} . This shift could be a consequence of the weakening of the hydrogen bonding between water and hydroxide layer due to the hydrophobicity of ionic liquid. This weakening of the bonds between water and hydroxide layer is in accordance to the findings on thermoanalysis, where the DSC

curve of Mg₃Al IL-US sample (Figure 2) suggested that the loss of interlayer water occurred at lower temperature. Due to the different synthesis mode, the Mg₃Al IL-COS sample, shows several changes in the FTIR spectrum (Figure 3d), as a consequence of the presence of ionic liquid in the interlayer space. The band at about 3500 cm⁻¹ is broader, probably due to the interaction between IL and the hydroxide layer, which causes the Mg-OH and Al-OH bonds to change their length. The doublet assigned to -CH₂- and -CH₃ groups in IL is found at 2932 cm⁻¹ and 2864 cm⁻¹. Due to this doublet, the band assigned to the carbonate-water bridging mode is not visible. Moreover, the band attributed to the bending mode of water molecules is found shifted to 1628 cm⁻¹ and a new shoulder situated at 1759 cm⁻¹ appears on the spectrum. The presence of this new shoulder can be explained by the presence of small amounts of coordinated water molecules to a cation [38]. This supposition is in accordance with the thermoanalytic studies, the DSC curve of Mg₃Al IL-COS sample showing a single endothermic peak due to the water loss, a sign of structural changes brought by the hydrophobic ionic liquid. Also, the presence of IL in the interlayer region is demonstrated by the shift of the band assigned to ν₂ vibration mode of carbonate group, from about 850 cm⁻¹ (in Mg₃Al and Mg₃Al IL-US samples) to 824 cm⁻¹, which could be explained by a change in the interaction between carbonate anion present in the interlayer space and the hydroxide layer. The endothermic shoulder at 480 °C found only on the DSC curve of the material (Figure 2), was attributed to the decarbonization process and could be a consequence of this change in the carbonate anion vibration mode.

The adsorption-desorption isotherms of the synthesized materials are presented in Figure 4. The BET surface areas calculated for this samples are presented in Table 1 and decrease as follows: Mg₃Al > Mg₃Al IL-US > Mg₃Al IL-COS. Regardless of the obtaining method, all isotherms belong to the Type IV according to IUPAC classification and belong to the H3 type of hysteresis loop. This kind of isotherm is associated with capillary condensation taking place in mesopores, does not exhibit any limiting adsorption at high p/p₀ and is observed with aggregates of plate-like particles giving rise to slit-shaped pores. A difference is observed, however, between materials Mg₃Al and Mg₃Al IL-US on the one hand, and material Mg₃Al IL-COS, on the other hand, in terms of N₂ volume adsorbed, which could be correlated to the pore diameter distribution. For samples Mg₃Al and Mg₃Al IL-US, the mesopores, with dimensions between 10 and 20 nm have major contributions to the textural properties, while the distribution range of the pore diameter of Mg₃Al IL-COS sample is wider, large mesopores and macropores (with dimensions between 30 and 70 nm) having the major contribution.

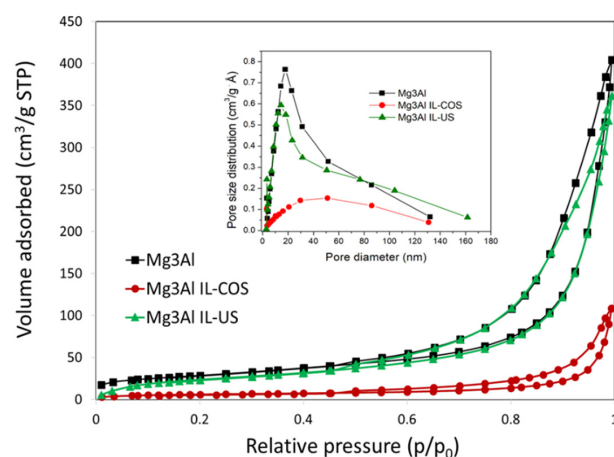


Figure 4. N₂ adsorption-desorption isotherms. Inlet: pore size distribution.

2.2. Kinetic Studies

The adsorption studies conducted at different stirring time led to the conclusions that the equilibrium between the Mg₃Al with or without Methyltrialkylammonium chloride and Pd(II) ions from the aqueous solutions, regardless of the work temperature, was achieved

quite fast, in 60 min. The dependence of the adsorption capacities developed by the studied adsorbent materials function of stirring time, at three different temperatures are presented in Figure 5. It is observed that the impregnated LDHs present a higher adsorption capacity than the raw LDH. In the case of non-functionalized Mg_3Al , at the working temperature of 298 K, a degree of 75.6% of Pd (II) ions recovering from solution is achieved, while in the case of the other two materials the removal efficiency is over 95%. The removal efficiency increases with the temperature increasing. Using the sample obtained through co-synthesis, a 100% removal efficiency is obtained at 313 K, and in case of the sample obtained through ultrasonication a complete removal efficiency is obtained at 328 K.

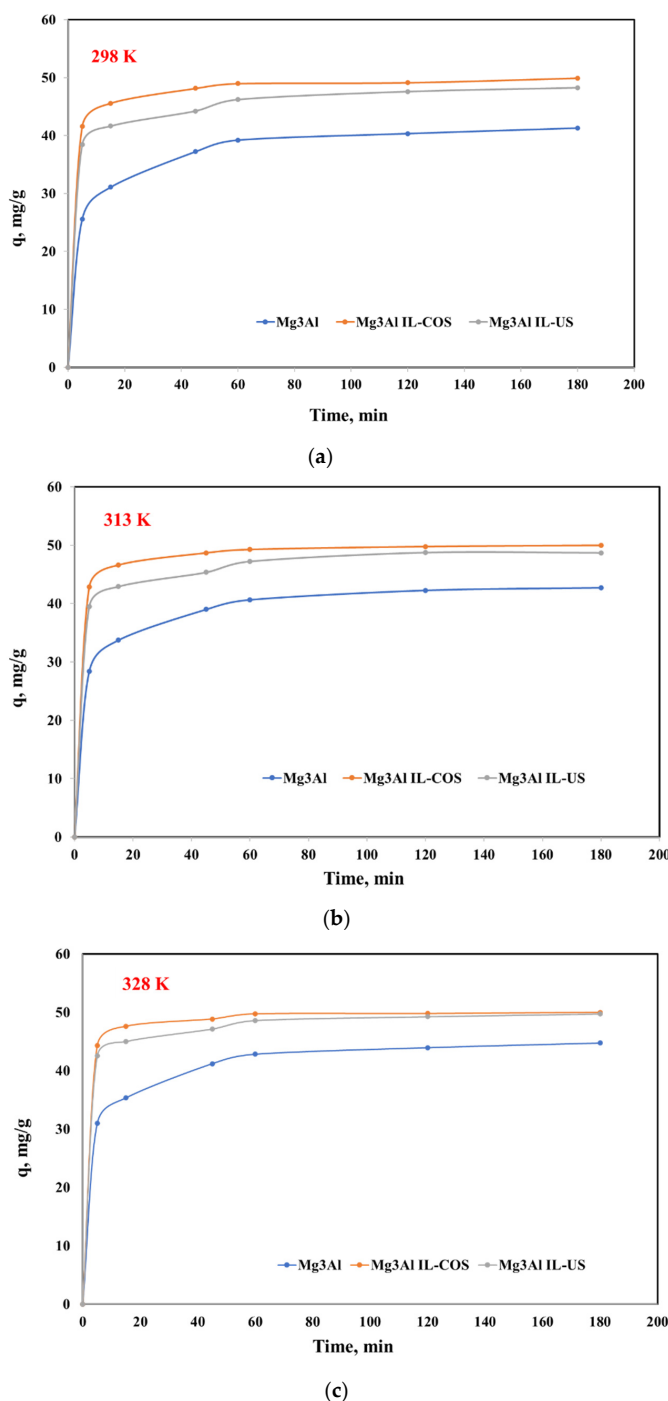


Figure 5. Effect of contact time on the adsorption capacity of studied LDHs in the adsorption process of Pd(II) ions from aqueous solutions at three different temperatures: (a) 298 K, (b) 313 K, (c) 328 K.

The experimental results were modelled with pseudo-first order, pseudo-second order and intra particle diffusion establish the rate limiting step and the type of adsorption mechanism.

The pseudo-first order model is expressed in its linear form, according to the following equation [40–42].

$$\ln(q_e - q_t) = \ln q_e - k_1 \cdot t \quad (1)$$

where: q_e and q_t represent the amount of Pd(II) adsorbed onto 1 g of adsorbent materials at equilibrium and after the treatment time, t ; k_1 represent the rate constant specific for the adsorption process of Pd ions onto studied materials.

The rate constant and the equilibrium adsorption capacity were determined from the slope and intercept of $\ln(q_e - q_t)$ versus stirring time (Figure 6).

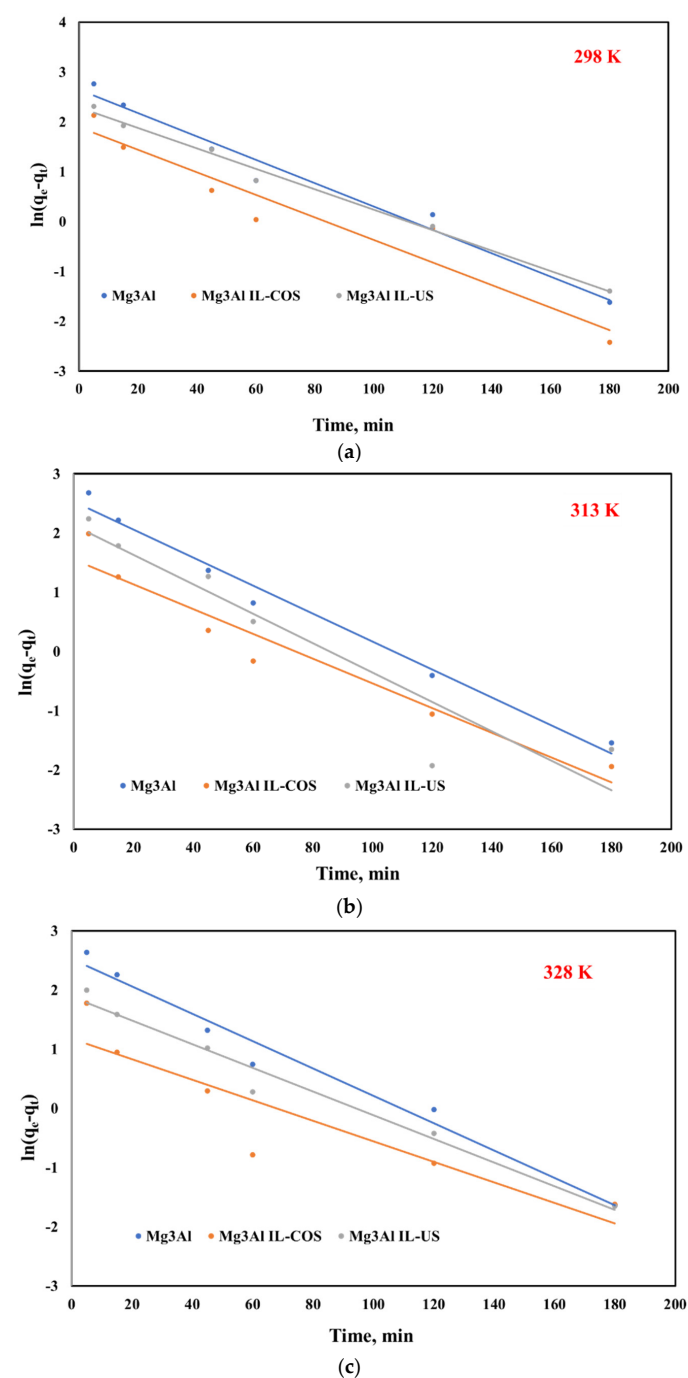


Figure 6. Pseudo-first order model for Pd(II) ions adsorption onto studied LDHs at three different temperatures: (a) 298 K, (b) 313 K, (c) 328 K.

If the process of Pd(II) adsorption onto the studied LDHs is controlled by the chemisorptions rate, then the experimental data are well modeled by the pseudo-second order kinetic model in its linear form:

$$\frac{t}{q_t} = \frac{1}{k_2 \cdot q_e^2} + \frac{t}{q_e} \quad (2)$$

where: q_e , q_t and t have the same significance as shown above, and k_2 is the rate constant of the pseudo-second order kinetic model.

These parameters could be determined from the slope and intercept of the linear plot between t/q_t and stirring time (Figure 7).

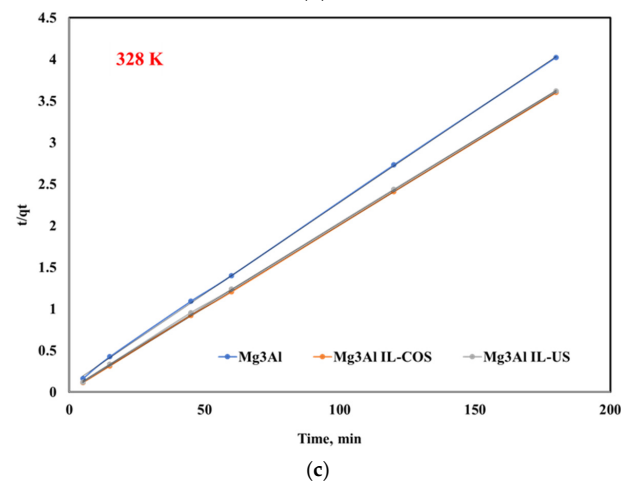
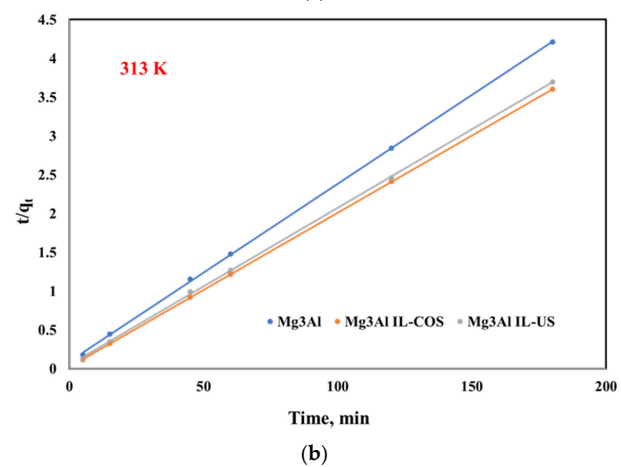
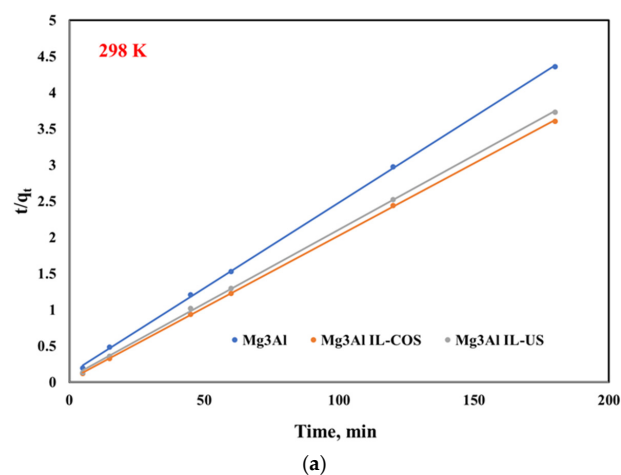
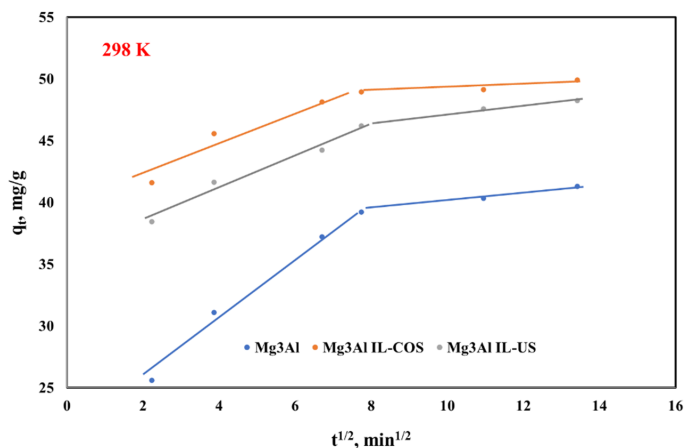


Figure 7. Pseudo-second order model for Pd(II) ions adsorption onto studied LDHs at three different temperatures: (a) 298 K, (b) 313 K, (c) 328 K.

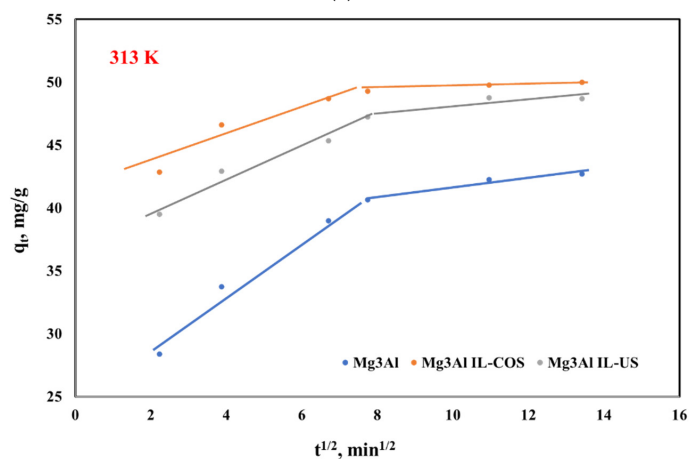
The rate limiting step in the process of adsorption of Pd ions onto studied LDHs could be established from the intraparticle diffusion experimental data model:

$$q_t = k_{in} \cdot t^{1/2} + C \tag{3}$$

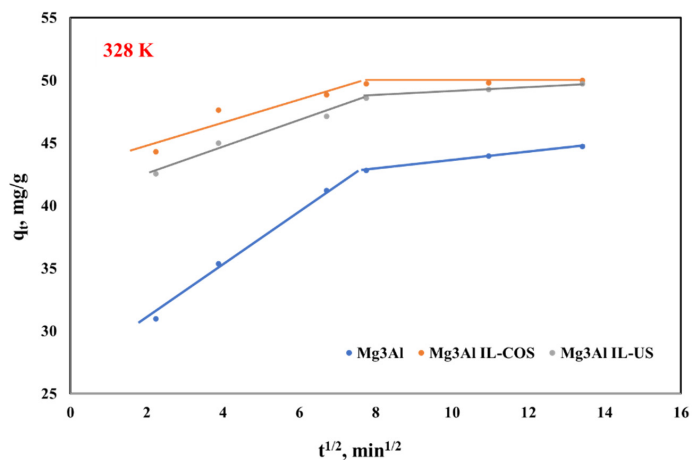
where: k_{in} represent the rate constant of the intraparticle diffusion model and was determined from the slope of the linear representation of q_t versus $t^{1/2}$ (Figure 8).



(a)



(b)



(c)

Figure 8. Intraparticle diffusion model for Pd(II) ions adsorption onto studied LDHs at three different temperatures: (a) 298 K, (b) 313 K, (c) 328 K.

The calculated rate constants, together with the obtained correlation coefficient are presented in Table 2.

Table 2. Kinetic models parameters for Pd(II) ions adsorption onto studied LDHs.

Adsorbent Material	Pseudo First Order				Pseudo Second Order			Intra Particle Diffusion		
	T = 298 K									
	q _e exp. mg/g	q _e calc. mg/g	K ₁ , min ⁻¹	R ²	q _e calc. mg/g	K ₂ · 10 ⁻³ , min/(mg/g)	R ²	K _{int} , mg/g min ^{-1/2}	C	R ²
Mg ₃ Al	41.3	13.1	0.0288	0.9769	42.2	0.0052	0.9996	1.9826	23.8	0.9966
Mg ₃ Al IL-COS	49.8	6.0	0.0218	0.9282	50.0	0.0139	0.999	0.9670	41.6	0.9943
Mg ₃ Al IL-US	48.2	9.1	0.0198	0.9929	48.8	0.0074	0.9997	0.9976	38.0	0.9701
T = 313 K										
	q _e exp.	q _e calc.	K ₁	R ²	q _e calc.	K ₂	R ²	K _{int}	C	R ²
Mg ₃ Al	42.7	12.5	0.0236	0.9837	43.7	0.0056	0.9998	1.2275	28.6	0.8383
Mg ₃ Al IL-COS	49.9	4.7	0.0209	0.9384	50.3	0.017	1	0.5635	43.6	0.7448
Mg ₃ Al IL-US	48.7	10.1	0.0248	0.8877	49.3	0.0086	0.9998	0.8110	39.3	0.8731
T = 328 K										
	q _e exp.	q _e calc.	K ₁	R ²	q _e calc.	K ₂	R ²	K _{int}	C	R ²
Mg ₃ Al	44.7	12.4	0.0231	0.9761	45.5	0.0058	0.9998	1.1962	30.9	0.8406
Mg ₃ Al IL-COS	50.0	3.3	0.0173	0.8254	50.3	0.0240	1	0.4379	45.1	0.7061
Mg ₃ Al IL-US	49.7	6.6	0.0200	0.9756	50.0	0.0110	0.9999	0.6200	42.4	0.8752

Data presented show that the kinetics of Pd(II) removal by adsorption on the studied material is described by a pseudo-second-order expression, because the correlation coefficient is very close to 1 and the theoretically predicted equilibrium sorption capacity is close to the value experimentally determined. This suggests that the rate-determining step may be chemical adsorption or chemisorption involving valence forces through sharing or exchange of electrons between adsorbent and adsorbate. For all the studied materials, the pseudo-second order constant rate, k_2 increases with the temperature increasing, suggesting that the Pd adsorption onto the studied materials is favored by the temperature increasing. This chemisorption process is a complex one, which takes place in two steps, according to the intraparticle diffusion plot (Figure 8). It is obvious that the intraparticle diffusion is not the rate-limiting step for adsorption of Pd(II) onto the studied LDH. In the first 10 min the Pd(II) diffuses through the solution until it reaches the LDHs surface, then the rate limiting step is controlled by the adsorption of the Pd(II) inside the particles of raw or functionalized Mg₃Al [43].

2.3. Thermodynamic Studies

To further elucidate if the Pd adsorption onto Mg₃Al-LDH and the samples functionalized with the studied ionic liquid, correspond to a physisorption or a chemisorption process, the activation energy was determined according to the Arrhenius equation described by the following equation:

$$\ln k = \ln A - \frac{E_a}{RT} \quad (4)$$

Activation energy in the adsorption process is the minimum energy needed of the adsorbate to interact with the functional groups on the adsorbent surfaces. If the interactions between the adsorbent and adsorbate involve weak forces, an activation energy below 4.2 kJ/mol is obtained meaning that a physisorption process takes place. If the interactions between the adsorbent and adsorbate involves stronger forces, higher values of E_a are obtained suggesting that a chemisorption process takes place [44,45]. The activation energy E_a for the adsorption process of Pd ions onto the studied materials were determined from the plot of $\ln k_2$ versus $1/T$ (Figure 9) and the results are presented in Table 3. It could be

observed that in case of Mg_3Al an activation energy of 2.97 kJ/mol is obtained, suggesting that Pd adsorption onto LDH take place only as physisorption in the materials pores.

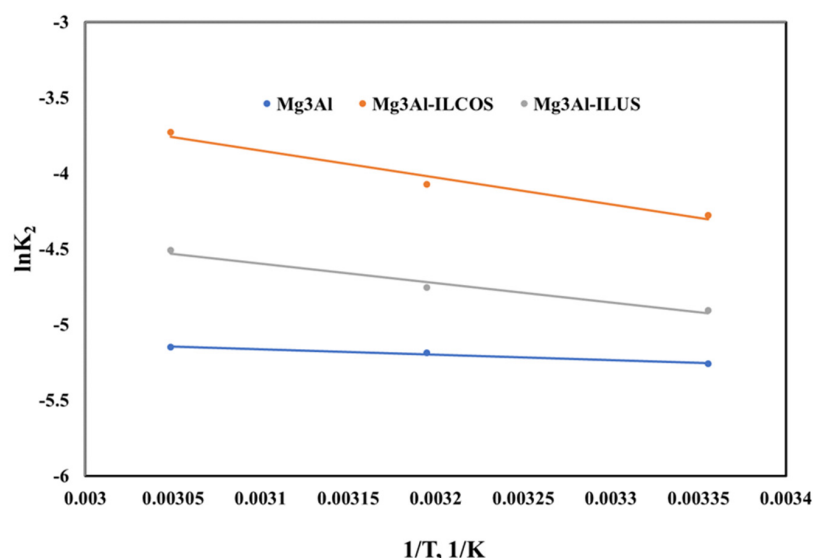


Figure 9. Arrhenius plot for Pd adsorption onto the studied LDHs.

Table 3. Thermodynamic parameters of Pd(II) adsorption onto the studied LDHs.

Adsorbent Material	E _a , kJ/mol	Thermodynamic Parameters					R ²
		ΔH ⁰ , kJ/mol ⁻¹	ΔS ⁰ , J/(mol K)	ΔG ⁰ , kJ/mol			
				298 K	313 K	328 K	
Mg ₃ Al	2.97	16.56	68.2	-3.87	-4.9	-5.93	0.9784
Mg ₃ Al IL-COS	14.72	65.38	272.2	-15.6	-19.7	-23.8	0.9983
Mg ₃ Al IL-US	10.68	46.98	185.9	-8.41	-11.2	-13.9	0.9926

In case of the LDH functionalized Methyltrialkylammonium chloride for the sample obtained through co-synthesis, an E_a = 14.72 kJ/mol is obtained, and for the one obtained through ultrasonication an E_a = 10.68 kJ/mol, respectively. In these cases, it is worth mentioning that the amino group introduced in the LDH structure contribute to the Pd recover from aqueous solutions involving stronger forces, and suggesting that Pd adsorption takes place due to a chemisorption process.

To conclude, if the Pd adsorption onto the studied LDHs is a spontaneous process or not, the Gibb's free energy (ΔG⁰) was determined, taking into consideration also the enthalpy (ΔH⁰) and the entropy (ΔS⁰) of the Pd adsorption process. The Gibb's free energy (ΔG⁰) was determined from the classical Van't Hoff equation [44,45].

$$\Delta G^0 = -RT \ln K_d \quad (5)$$

$$\Delta G^0 = \Delta H^0 - T \Delta S^0 \quad (6)$$

K_d, the equilibrium constant, could be determined at different temperature by the following equation:

$$K_d = \frac{q_e}{C_e} \quad (7)$$

The thermodynamic parameters of ΔH⁰ and ΔS⁰ were calculated from the linear regression according to the following equation represented in Figure 10:

$$\ln K_d = \frac{\Delta S^0}{R} - \frac{\Delta H^0}{RT} \quad (8)$$

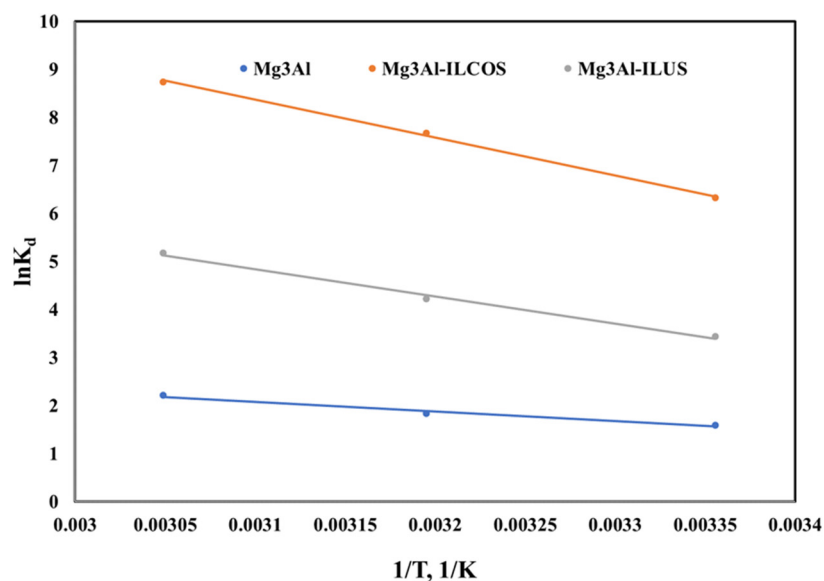


Figure 10. Effect of temperature on Pd adsorption onto the studied LDHs.

The obtained thermodynamic parameters are listed in Table 3.

From the data presented in Table 3, for all the studied LDHs the positive values of enthalpy indicate the endothermic nature of Pd(II) adsorption. The values obtained for Gibbs free energy are negative and increase in module with the temperature increasing suggesting that the Pd(II) adsorption onto the studied LDHs is a spontaneous processes. For the entropy, a positive value was obtained suggesting an increase in randomness at the solid/liquid interface during adsorption of Pd(II) ions onto the studied LDHs.

2.4. Equilibrium Studies

The maximum adsorption capacity of raw and functionalized Mg₃Al developed for the recovery process of Pd(II) from aqueous solutions could be experimentally determined from the equilibrium isotherm presented in Figure 11. It can be observed that the adsorption capacity of the studied materials increase with the equilibrium concentration of Pd(II) ions from the aqueous solutions. The adsorption capacity developed by the functionalized Mg₃Al is almost two times higher (in case of the co-synthesis—Mg₃Al IL-COS) than those developed by the raw Mg₃Al.

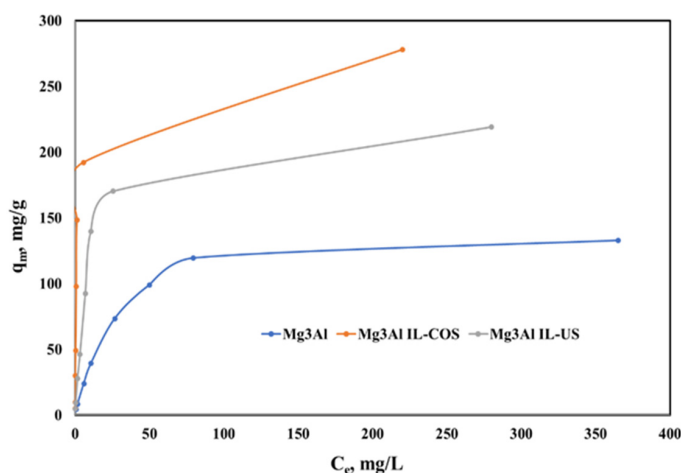


Figure 11. Equilibrium isotherms of Pd(II) ions adsorption onto studied LDHs.

Three isotherm models, based on two parameters (Langmuir, Freundlich and Temkin) were applied to model the equilibrium data obtained experimentally.

The linearized Langmuir isotherm represented by the following equation suggests that the Pd(II) adsorption onto studied LDHs occurs as a monolayer, covering the adsorbent surface:

$$\frac{C_e}{q_e} = \frac{1}{q_m \cdot K_L} + \frac{C_e}{q_m} \tag{9}$$

where: q_m represents the maximum adsorption capacity developed by the studied LDHs and K_L represents the Langmuir constant. These two parameters can be determined from the linear plot of C_e/q_e versus C_e (Figure 12).

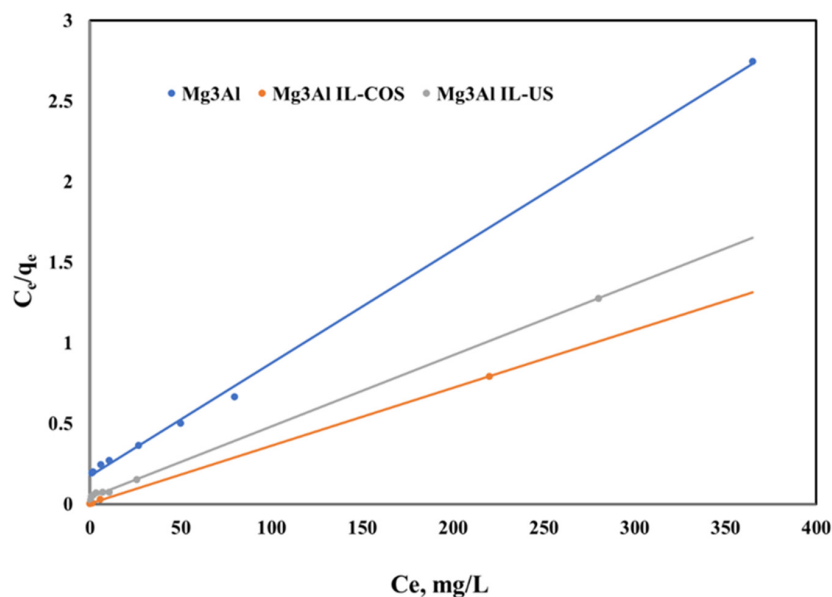


Figure 12. Langmuir isotherms of Pd(II) ions adsorption onto studied LDHs.

The affinity between the raw Mg_3Al or functionalized Mg_3Al and the Pd(II) ions can be obtained by fitting the data to the linearized form of the Freundlich isotherm:

$$\ln(q_e) = \ln(k_F) + \frac{1}{n} \ln(C_e) \tag{10}$$

where: $1/n$ and the Freundlich constant k_F represent the Freundlich isotherms parameters and can be determined from the plot of $\ln(q_e)$ versus $\ln(C_e)$ presented in Figure 13.

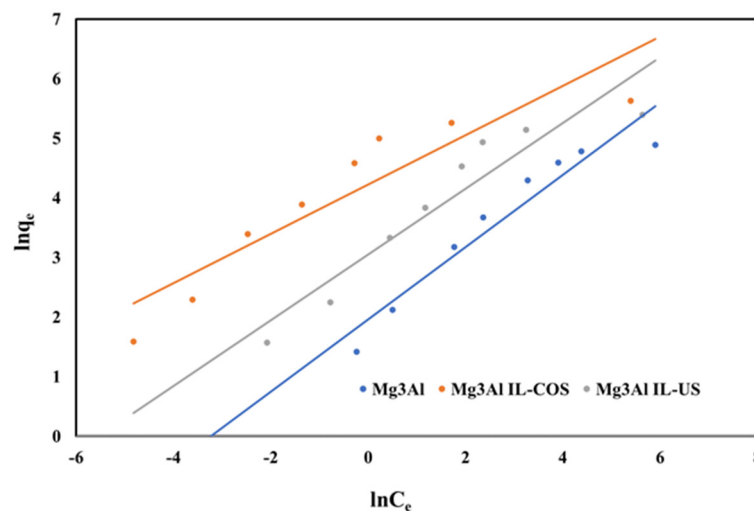


Figure 13. Freundlich isotherms of Pd(II) ions adsorption onto studied LDHs.

If the surface of the adsorbent is heterogeneous, the equilibrium data will present a good fit for the linearized form of the Temkin isotherm model, which is given by the next equation, suggesting that the heat of adsorption decreases during the adsorption process:

$$q_e = \frac{R \cdot T}{b} \ln k_T + \frac{R \cdot T}{b} \ln(C_e) \quad (11)$$

where: k_T is the equilibrium binding constant, and b is related to the heat of adsorption, which were determined from the linear plot between q_e and $\ln(C_e)$ presented in Figure 14.

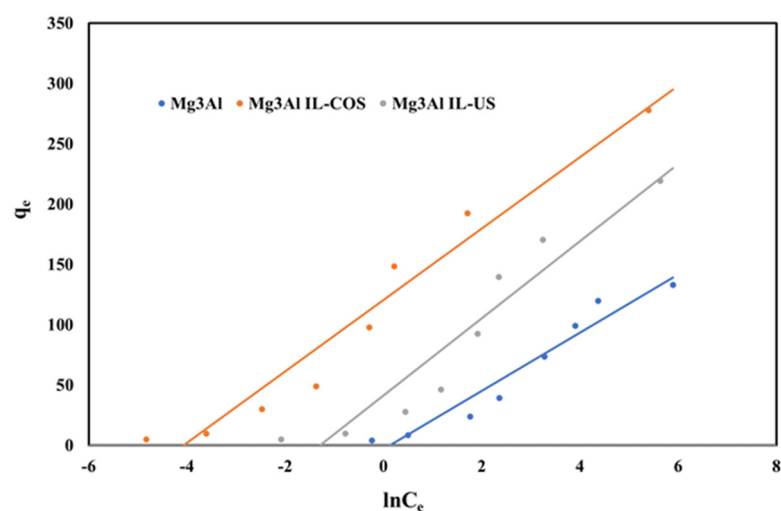


Figure 14. Temkin isotherms of Pd(II) ions adsorption onto studied LDHs.

The equilibrium parameters together with the obtained correlation coefficient are presented in Table 4.

Table 4. Equilibrium sorption isotherm parameters for Pd(II) ions adsorption onto studied LDHs.

		Mg ₃ Al	Mg ₃ Al IL-COS	Mg ₃ Al IL-US
Equilibrium isotherm	q_m , exp, mg/g	132.9	277.8	219.1
	q_m , calc, mg/g	142.9	277.7	227.3
Langmuir	K_L , L/mg	0.0399	0.8782	0.1073
	R^2	0.9987	0.9999	0.9994
	$1/n$	0.6063	0.4135	0.5508
Freundlich	K_F , mg/g	7.11	68.3	21.2
	R^2	0.9214	0.8515	0.8926
Temkin	b , J/mol	102.8	83.7	77.6
	K_T , L/g	0.872	58.8	3.63
	R^2	0.9432	0.9536	0.91

It could be observed that the Langmuir isotherm better describes the adsorption process of Pd(II) ions onto the studied material, as compared with other isotherm models due to the values of the obtained correlation coefficients, which are close to 1. Moreover, the maximum adsorption capacity of the studied material obtained from the Langmuir plot is very close to that obtained experimentally. The Langmuir model assumes that the surface of the adsorbent is homogenous and the sorption energy to be equivalent for each sorption site. Due to the fact that the Langmuir isotherm fits the experimental data better than the other isotherm types, it can be mentioned that the Pd(II) ions are adsorbed uniform onto the surface of the studied adsorbent, because of the homogenous distribution of active site onto the surface. In this case there is no migration of the palladium ions onto the surface of

the studied adsorbent, suggesting a possible chemisorption process between the adsorbent and adsorbate.

2.5. Mechanism of Palladium Adsorption onto the Studied Materials

Correlating the results from the characterization section with the results obtained from kinetic, thermodynamic and equilibrium studies the following mechanism of palladium adsorption onto the studied materials could be proposed (Figure 15).

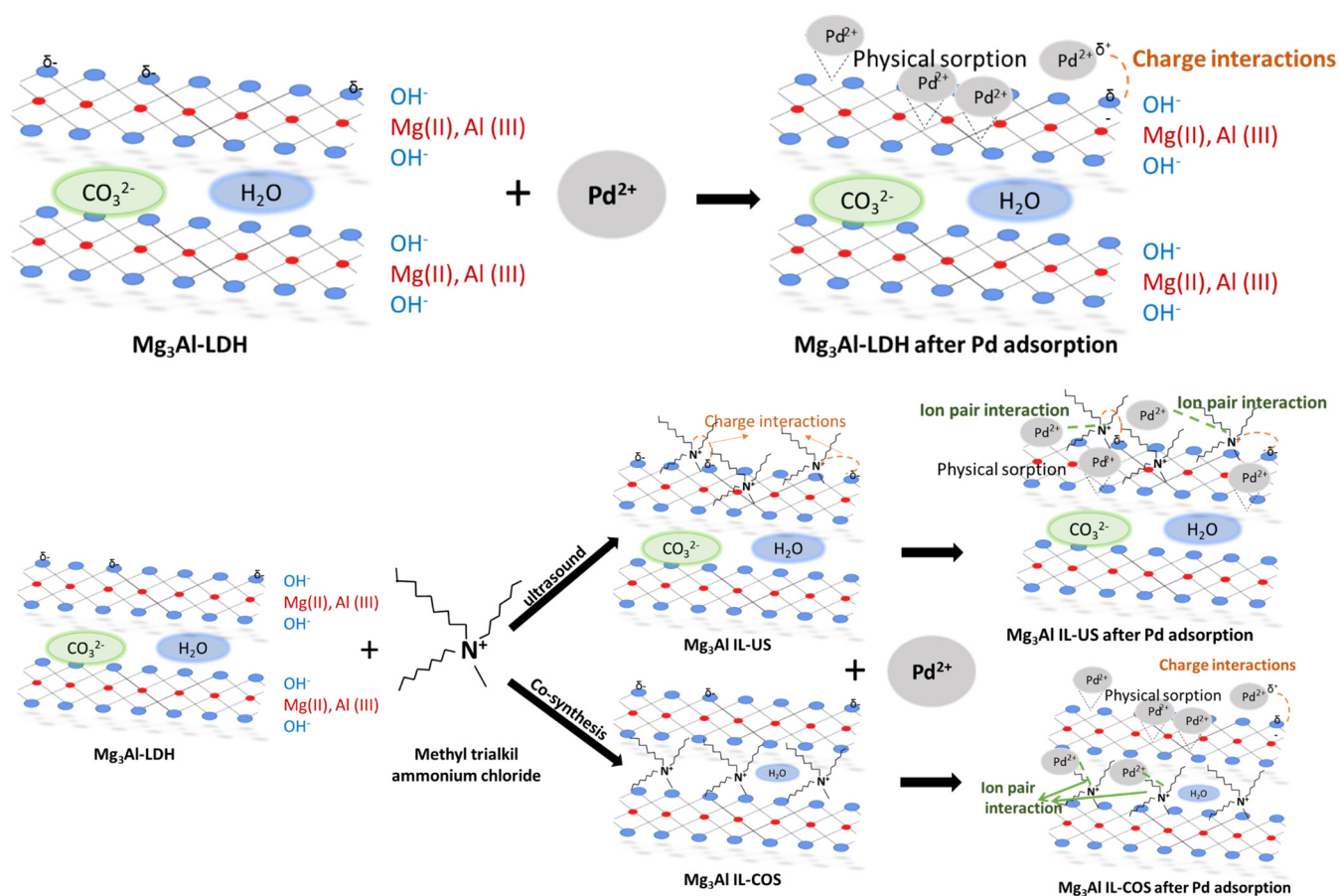


Figure 15. Adsorption mechanism of Pd ions onto the studied materials.

In case of Mg₃Al, the Pd adsorption took place on the surface of the LDH, in pores or through electrostatic interactions between the Pd ions and the hydroxyl ions present on the surface of the LDH. This physical sorption of Pd recover from aqueous solutions, using Mg₃Al as adsorbent material, is confirmed by the low value of activation energy, 2.97 kJ/mol, resulted from the thermodynamic study.

In case of the functionalized Mg₃Al samples with Methyltrialkylammonium chloride obtained higher adsorption capacities due to the interaction of Pd ions, with the functional groups from the studied IL structure. As can be seen from Figure 15 could appear ion-pair interaction between the Pd (which is found under palladium chloride) and the quaternary ammonium from the studied IL. These results are in agreement with other studies presented in literature [46–49]. It is also well known that the interaction between palladium ions and quaternary ammonium is highly used in the formation of stable complex which are used as catalyst in various chemical processes [50,51]. Therefore, the samples functionalized with Methyltrialkylammonium chloride developed higher adsorption capacities and higher values for activation energy. All the results from thermodynamic, kinetic and equilibrium studies underline the chemisorption process which describes the palladium recover from aqueous solutions onto Mg₃Al IL-US, and Mg₃Al IL-COS.

It could be observed that the synthesis method used for the adsorbent obtaining also influenced the adsorption capacity developed by the studied materials in the recovery process of palladium ions from aqueous solutions. The highest adsorption capacity is developed by the sample functionalized through co-synthesis. In this case, as the adsorption of palladium ions contribute as a synergic effect both the ionic liquid and also the Mg₃Al-LDH. In this case the ionic liquid is found in the interlayer of the Mg₃Al-LDH, and Pd ions are retained by the ion-pair and charge interaction with the IL, but also by physical sorption onto the surface of the LDH. In case of the sample obtained through ultrasound method, because the ionic liquid is found on the surface of the Mg₃Al-LDH and not in the interlayer space, the Pd ions are retained by the interaction between the IL and it, but the adsorption process is decreased, because the loading of IL onto the surface of LDH decrease the available site for the Pd physical sorption.

2.6. Comparison of the Adsorption Capacity Developed by the Studied Materials with other Materials Reported in Literature

Comparing the maximum adsorption capacities developed by the studied adsorbents with the adsorption capacities of other materials, reported in literature, it could be concluded that the Mg₃Al-LDH presents a higher efficiency, especially if it is functionalized with ionic liquid, in the removal process of Pd ions from aqueous solutions (Table 5).

Table 5. Comparison of some of the selected diverse adsorbents reported in recent literature.

Adsorbent	q _m , mg/g	References
2-Mercaptobenzothiazole functionalized Amberlite XAD-1180 resin	50.0	[46]
Silica-based adsorbent functionalized with macrocyclic ligand	83.0	[47]
Aliquat-336 (ionic liquid) impregnated onto chitosan	187.61	[48]
Tetraoctylammonium bromide impregnated onto graphene oxide	92.67	[49]
MgSiO ₃ functionalized with DL-cysteine	9.23	[52]
Zn ₃ Al	64.4	[23]
Zn ₃ Al-IL	100	
Zn ₃ Al-ILUS	92.4	
Mg ₃ Al	142.9	Present paper
Mg ₃ Al IL-COS	277.8	
Mg ₃ Al IL-US	227.3	

The comparison of the adsorption capacities developed by the synthesized and characterized materials was made with other similar materials. It is observed that other researchers were also focused on the use of some functionalized materials and used ammonium as functional group. It was used the same ionic liquids Aliquat-336, but impregnated onto chitosan [48], or Zn₃Al [23]. In these cases, we obtained an adsorption capacity of 187.61 mg/g and 100 mg/g, respectively, compared with the q_{max} = 277.3 mg/g developed by Mg₃Al IL-COS. These results suggested that both the ionic liquid and also the support materials contribute as a synergic effect to the recovery of palladium ions from aqueous solutions. Another important result reported in the literature is the case of the use of tetraoctylammonium bromide impregnated onto graphene oxide. In this case, an adsorption capacity of 92.67 mg/g is obtained, suggesting the important role of the ammonium functional group in the recover process of Pd ions from aqueous solution due to the formation of the strong interactions between these two. Other reported materials present much more lower adsorption capacities, underlying one more time the importance of the properties of the used solid support and the efficiency demonstrated by the ammonium group.

3. Materials and Methods

3.1. Adsorbent Materials Obtaining and Characterization

The layered double hydroxide used in this study was synthesized by co-precipitation method using as precursors $\text{Mg}(\text{NO}_3)_2 \cdot 6\text{H}_2\text{O}$ and $\text{Al}(\text{NO}_3)_3 \cdot 9\text{H}_2\text{O}$. The ratio between the cation in the LDH was calculated to be $\text{Mg}:\text{Al} = 3:1$. 200 mL of 1 M solution containing the nitrates salts in the desired metal ions ratio was prepared and added gradually, under vigorous stirring in a volume of 100 mL of 1M Na_2CO_3 solution. A 2M NaOH solution was used to maintain the suspension pH around 10.5 value. To obtain the Mg_3Al -LDH, the suspension was subject to maturation for 24 h at 70 °C. The obtained precipitate was filtered, washed, crushed, sieved, and used in the further experiments. A part of the obtained Mg_3Al was functionalized with the studied ionic liquid through ultrasound method, which was described in our previously published papers [23,53]. The obtained sample, symbolized Mg_3Al IL-US, was prepared with 10% IL addition. For the second method of functionalization by co-synthesis, the studied ionic liquid was introduced in the stage of the LDH co-precipitation (Mg_3Al IL-COS), by replacing the Na_2CO_3 solution with the IL previously dissolved in acetone [23]. The further steps of sample preparation were maintained. The obtained adsorbent materials were subjected to structural and morphological characterization using X-ray diffraction (XRD), N_2 adsorption-desorption analysis, Fourier-transform infrared (FTIR) spectroscopy and by thermal analysis. The XR diffractograms were obtained by using a Rigaku Ultima IV X-ray diffractometer (40 kV, 40 mA) with $\text{Cu}_{\text{K}\alpha}$ radiation. The N_2 adsorption-desorption experiments were developed at 77 K by using a Micromeritics ASAP 2020 instrument, after degassing the samples for 48 h at 100 °C, under 8 μmHg vacuum. The specific surface area was calculated using the BET method and the pore size distribution was calculated using the BJH method based on the N_2 desorption isotherm. The FTIR spectra of the samples were recorded using a Shimadzu IR Prestige-21 FTIR spectrophotometer in the range 400–4000 cm^{-1} and a nominal resolution of 4 cm^{-1} , the samples being prepared as pellets by mixing with KBr. Thermal analysis was performed by using a Netzsch STA 449C equipment. Differential scanning calorimetry (DSC) and thermogravimetric (TG) curves were obtained by heating the materials in the temperature range 25–1000 °C, with a heating rate of 10 °C/min under air flow.

3.2. Pd Recover from Aqueous Solutions

The obtained Mg_3Al -LDH with or without Methyltrialkylammonium chloride were used as adsorbent materials in the recovery process of Pd ions from aqueous solutions. The adsorption of palladium (II) ions was performed in batch mode. The efficiency of raw or impregnated Mg_3Al -LDH was determined by studying the dependence of their developed adsorption capacity function of stirring time and initial concentration of Pd ions from aqueous solutions. From the literature survey it was concluded that the Pd ions are better adsorbed at pH values lower than 4 [53–56]. Therefore, in this paper all the adsorption studies were performed using Pd solutions with an initial pH around 3.6, the lowest possible pH to avoid the LDH dissolution. To determine the time when the equilibrium between the adsorbent and adsorbate is established, adsorption experiments were performed using different times (5–180 min) for stirring the reaction mixture, which consists of 25 mL of 50 mg/L Pd(II) solutions and 0.025 g of adsorbent materials. The kinetic studies were performed at three different temperatures (298 K, 313 K and 328 K). To determine the efficiency of the studied materials in the recovery process of Pd ions from aqueous solutions, their maximum adsorption capacity was established by performing equilibrium studies. In this way, the adsorption studies were conducted using Pd(II) solutions containing different initial concentrations (5–500 mg/L Pd(II)). The equilibrium studies were performed using the same initial pH of Pd solutions, the same solid:liquid ratio, S:L = 1:1, and a stirring time of 60 min. After stirring the mass reaction, the samples were filtered and in the resulted solutions the residual concentration of Pd(II) ions was

determined through atomic absorption spectrophotometry, using an atomic absorption spectrophotometer Varian SpectrAA 280 FS.

The adsorption efficiency of the studied materials was expressed by the amount of Pd ions adsorbed on 1 g of adsorbent according to the following equation:

$$q_e = \frac{(C_0 - C_e)V}{m} \quad (12)$$

where: q_e —equilibrium capacity developed by adsorbent materials, mg Pd/g adsorbent material.

- C_0 —initial concentration of Pd(II) in aqueous solutions, mg/L.
- C_e —equilibrium concentration of Pd(II), mg/L.
- V —volume of the solution containing Pd(II) used in the adsorption process, L.
- m —mass of adsorbent material used in the adsorption process, g.

4. Conclusions

In the present work, Mg_3Al -type layered double hydroxide was synthesized and functionalized by two methods (co-synthesis and ultrasonication), with ionic liquid (Methyltrialkylammonium chloride). X-ray diffraction, FTIR, BET and thermal analysis confirmed the formation of the Mg_3Al -type layered double hydroxide.

By its functionalization by co-synthesis, IL is observed to be located between the LDH layers, and by the ultrasound method IL is found on the LDH surface.

The synthesized and characterized materials were used in the recovery process of Pd(II) ions from aqueous solutions. The adsorption capacity increases with the increasing contact time, increasing temperature and increasing equilibrium concentration of Pd(II). The presence of ionic liquid significantly improves the efficiency of Mg_3Al in the recovery process of Pd(II) ions from aqueous solutions.

The adsorption kinetics were better described by the pseudo-second-order kinetic model compared to the pseudo-first-order kinetic model.

The experimental data showed a good fit with the Langmuir isotherm.

The adsorption capacity increases as follows: $Mg_3Al \ll Mg_3Al \text{ IL-US} < Mg_3Al \text{ IL-COS}$.

By correlating the results obtained in the characterization process of adsorbent materials with the results obtained from kinetic, thermodynamic and equilibrium studies, we can conclude that in the case of the raw Mg_3Al sample, Pd recovery occurs through a physisorption mechanism, as it is adsorbed in the pores of the material. In contrast, in the case of IL (Methyltrialkylammonium chloride) functionalized samples, Pd recovery is due to a chemisorption process, indicating that the functional groups of the ionic liquid confer a beneficial influence on the adsorbent material. This is very important for the future perspective of using and reclaiming of the exhausted adsorbent as photocatalyst in the degradation process of organic compounds from waters. Additionally, as a future experiment, the column adsorption test will be conducted in order to optimize the recovery process of the Pd ions from aqueous solutions and in order to obtain a higher quantity of the photocatalysts. The use of exhausted adsorbent as a photocatalyst could close the life cycle of products through sustainable consumption and production by improving waste management with greater recycling and reuse to create benefits for the environment, the economy and society.

Author Contributions: Conceptualization, L.C. and L.L.; Data curation, L.C. and N.S.T.; Formal analysis, N.S.T.; Investigation, L.L., N.S.T. and R.L.; Methodology, L.C., L.L. and R.P.; Resources, L.L.; Software, R.L.; Supervision, R.P.; Validation, R.L.; Visualization, L.C., L.L. and R.L.; Writing—original draft, L.C. and L.L. All authors have read and agreed to the published version of the manuscript.

Funding: This research was funded by Romanian Ministry of Education and Research, CNCS—UEFISCDI grant number PN-III-P1-1.1-TE-2019-1555, within PNCDI III.

Conflicts of Interest: The authors declare no conflict of interest.

References

1. European Commission. *Report on Critical Raw Materials in the Circular Economy*; European Commission: Brussels, Belgium, 2018.
2. Zhang, B.; Fu, L.; Wang, S.; Zhang, L. Adsorption of palladium (II) from aqueous solution using nanosilica modified with imidazoline groups. *Mater. Chem. Phys.* **2018**, *214*, 533–539. [[CrossRef](#)]
3. Trucillo, P.; Di Maio, E.; Lancia, A.; Di Natale, F. Selective Gold and Palladium Adsorption from Standard Aqueous Solutions. *Processes* **2021**, *9*, 1282. [[CrossRef](#)]
4. Nagarjuna, R.; Sharma, S.; Rajesh, N.; Ganesan, R. Effective Adsorption of Precious Metal Palladium over Polyethyleneimine-Functionalized Alumina Nanopowder and Its Reusability as a Catalyst for Energy and Environmental Applications. *ACS Omega* **2018**, *2*, 4494–4504. [[CrossRef](#)] [[PubMed](#)]
5. Maranescu, B.; Lupa, L.; Mihali, M.T.-L. Synthesis, characterizations and Pb(II) sorption properties of cobalt phosphonate materials. *Pure Appl. Chem.* **2016**, *88*, 979–992. [[CrossRef](#)]
6. Wojnicki, M.; Socha, R.P.; Pędzich, Z.; Mech, K.; Tokarski, T.; Fitzner, K. Palladium(II) Chloride Complex Ion Recovery from Aqueous Solutions Using Adsorption on Activated Carbon. *J. Chem. Eng. Data* **2018**, *63*, 702–711. [[CrossRef](#)]
7. Limin, Z.; Jinhui, L.; Zhirong, L. Adsorption of platinum (IV) and palladium (II) from aqueous solution by thiourea-modified chitosan microspheres. *J. Hazard. Mater.* **2009**, *172*, 439–446.
8. Sharififard, H.; Ashtiani, F.Z.; Soleimani, M. Adsorption of palladium and platinum from aqueous solutions by chitosan and activated carbon coated with chitosan. *Asia-Pac. J. Chem. Eng.* **2012**, *8*, 384–395. [[CrossRef](#)]
9. Sharma, R.; Arizaga, G.G.C.; Saini, A.K.; Shandilya, P. Layered double hydroxide as multifunctional materials for environmental remediation: From chemical pollutants to microorganisms. *SM&T* **2021**, *29*, e00319.
10. Mishra, G.; Dash, B.; Pandey, S. Layered double hydroxides: A brief review from fundamentals to application as evolving biomaterials. *Appl. Clay Sci.* **2018**, *153*, 172–186. [[CrossRef](#)]
11. Tang, Z.; Qiu, Z.; Lu, S.; Shi, X. Functionalized layered double hydroxide applied to heavy metal ions absorption: A review. *Nanotechnol. Rev.* **2020**, *9*, 800–819. [[CrossRef](#)]
12. Ishak, S.N.; Nizam Nik Malek, N.A. Functionalized layered double hydroxide with compound to remove cationic and anionic pollutants: A review. *Environ. Toxicol. Manag.* **2021**, *1*, 26–29. [[CrossRef](#)]
13. Tamilarasan, P.; Ramaprabhu, S. Ionic liquid functionalization—An effective way to tune carbon dioxide adsorption properties of carbon nanotubes. *RSC Adv.* **2015**, *5*, 35098–35106. [[CrossRef](#)]
14. Erto, A.; Silvestre-Albero, A.; Silvestre-Albero, J.; Rodríguez-Reinoso, F.; Balsamo, M.; Lancia, A.; Montagnaro, F. Carbon-supported ionic liquids as innovative adsorbents for CO₂ separation from synthetic flue-gas. *J. Colloid Interface Sci.* **2015**, *448*, 41–50. [[CrossRef](#)] [[PubMed](#)]
15. Zarezadeh-Mehrzi, M.; Badieli, A.; Mehrabadi, A.R. Ionic liquid functionalized nanoporous silica for removal of anionic dye. *J. Mol. Liq.* **2013**, *180*, 95–100. [[CrossRef](#)]
16. Zambare, R.; Song, X.; Bhuvana, S.; Antony Prince, J.S.; Nemade, P. Ultrafast Dye Removal Using Ionic Liquid–Graphene Oxide Sponge. *ACS Sustain. Chem. Eng.* **2017**, *5*, 6026–6035. [[CrossRef](#)]
17. Lupa, L.; Negrea, P.; Popa, A. *Use of Ionic Liquids in Solid-Liquid Separation Processes, Progress and Developments in Ionic Liquids*, Scott Handy; IntechOpen: London, UK, 2017.
18. Wieszczycka, K.; Filipowiak, K.; Wojciechowska, I.; Aksamitowski, P. Novel ionic liquid-modified polymers for highly effective adsorption of heavy metals ions. *Sep. Purif. Technol.* **2020**, *236*, 116313. [[CrossRef](#)]
19. Bujok, S.; Konefał, M.; Abbrent, S.; Pavlova, E.; Svoboda, J.; Trhlikova, O.; Beneš, H. Ionic liquid-functionalized LDH as catalytic-initiating nanoparticles for microwave-activated ring opening polymerization of ϵ -caprolactone. *React. Chem. Eng.* **2020**, *5*, 506–518. [[CrossRef](#)]
20. Bujok, S.; Hodan, J.; Beneš, H. Effects of Immobilized Ionic Liquid on Properties of Biodegradable Polycaprolactone/LDH Nanocomposites Prepared by In Situ Polymerization and Melt-Blending. *Nanomaterials* **2020**, *10*, 969. [[CrossRef](#)] [[PubMed](#)]
21. Alhumaimess, M.S.; HotanAlsohaimi, I.; Hassan, H.M.A.; El-Sayed, M.Y.; Alshammari, M.S.; Aldosari, O.F.; Kamel, M.M. Synthesis of ionic liquid intercalated layered double hydroxides of magnesium and aluminum: A greener catalyst of Knoevenagel condensation. *J. Saudi Chem. Soc.* **2020**, *24*, 321–333. [[CrossRef](#)]
22. Pizzoferrato, R.; Ciotta, E.; Ferrari, I.V.; Narducci, R.; Pasquini, L.; Varone, A.; Di Vona, M.L. Layered Double Hydroxides Containing an Ionic Liquid: Ionic Conductivity and Use in Composite Anion Exchange Membranes. *ChemElectroChem* **2018**, *5*, 2781–2788. [[CrossRef](#)]
23. Cochechi, L.; Lupa, L.; Țolea, N.S.; Muntean, C.; Negrea, P. Sequential use of ionic liquid functionalized Zn-Al layered double hydroxide as adsorbent and photocatalyst. *Sep. Purif. Technol.* **2020**, *250*, 117104. [[CrossRef](#)]
24. Cui, H.; Chen, J.; Yang, H.; Wang, W.; Liu, Y.; Zou, D.; Liu, W.; Men, G. Preparation and application of Aliquat 336 functionalized chitosan adsorbent for the removal of Pb(II). *Chem. Eng. J.* **2013**, *232*, 372–379. [[CrossRef](#)]
25. Ranjbari, S.; Tanhaei, B.; Ayati, A.; Sillanpää, M. Novel Aliquat-336 impregnated chitosan beads for the adsorptive removal of anionic azo dyes. *Int. J. Biol. Macromol.* **2018**, *125*, 989–998. [[CrossRef](#)]

26. Lupa, L.; Coheci, L.; Pode, R.; Hulka, I. Phenol adsorption using Aliquat 336 functionalized Zn-Al layered double hydroxide. *Sep. Purif. Technol.* **2017**, *196*, 82–95. [[CrossRef](#)]
27. Wei, W.; Song, M.H.; Kim, S.; Bediako, J.K.; Yun, Y.S. Selective Recovery of Au(III) from Binary Metal Solution Using Aliquat-336-Impregnated Alginate Capsule. *AMR* **2015**, *1130*, 511–514. [[CrossRef](#)]
28. Wiyantoko, B.; Kurniawati, P.; Purbaningias, T.E.; Fatimah, I. Synthesis and Characterization of Hydrotalcite at Different Mg/Al Molar Ratios. *Procedia Chem.* **2015**, *17*, 21–26. [[CrossRef](#)]
29. Macala, G.S.; Robertson, A.W.; Day, Z.B.; Lewis, R.S.; Iretskii, A.V.; Ford, P.C. Transesterification Catalysts from Iron Doped Hydrotalcite-like Precursors: Solid Bases for Biodiesel Production. *Catal. Lett.* **2008**, *122*, 205–209. [[CrossRef](#)]
30. Kwon, D.; Kang, J.Y.; An, S.; Yang, I.; Jung, J.C. Tuning the base properties of Mg–Al hydrotalcite catalysts using their memory effect. *J. Energy Chem.* **2020**, *46*, 229–236. [[CrossRef](#)]
31. Dietmann, K.M.; Linke, T.; del Nogal Sánchez, M.; Pérez Pavón, J.L.; Rives, V. Layered Double Hydroxides with Intercalated Permanganate and Peroxydisulphate Anions for Oxidative Removal of Chlorinated Organic Solvents Contaminated Water. *Minerals* **2020**, *10*, 462. [[CrossRef](#)]
32. Dietmann, K.M.; Linke, T.; Trujillano, R.; Rives, V. Effect of Chain Length and Functional Group of Organic Anions on the Retention Ability of MgAl-Layered Double Hydroxides for Chlorinated Organic Solvents. *ChemEngineering* **2019**, *3*, 89. [[CrossRef](#)]
33. Villegas, J.C.; Giraldo, O.H.; Laubernds, K.; Suib, S.L. New Layered Double Hydroxides Containing Intercalated Manganese Oxide Species: Synthesis and Characterization. *Inorg. Chem.* **2003**, *42*, 5621–5631. [[CrossRef](#)] [[PubMed](#)]
34. Tolea, N.S.; Coheci, L.; Lupa, L.; Voda, R.; Pode, R. Development of New Efficient Adsorbent by Functionalization of Mg 3 Al-LDH with Methyl Trialkyl Ammonium Chloride Ionic Liquid. *Molecules* **2021**, *26*, 7384. [[CrossRef](#)] [[PubMed](#)]
35. Stanimirova, T.; Vergilov, I.; Kirov, G.; Petrova, N. Thermal decomposition products of hydrotalcite-like compounds: Low-temperature metaphases. *J. Mater. Sci.* **1999**, *34*, 4153–4161. [[CrossRef](#)]
36. Kozak, M.; Domka, L. Adsorption of the quaternary ammonium salts on montmorillonite. *J. Phys. Chem. Solids* **2004**, *65*, 441–445. [[CrossRef](#)]
37. Klopogge, J.T.; Frost, R.L. Fourier Transform Infrared and Raman Spectroscopic Study of the Local Structure of Mg-, Ni-, and Co-Hydrotalcites. *J. Solid State Chem.* **1999**, *146*, 506–515. [[CrossRef](#)]
38. Labajos, F.M.; Rives, V.; Ulibarri, M.A. Effect of hydrothermal and thermal treatments on the physicochemical properties of IVIg-Al hydrotalcite-like materials. *J. Mat. Sci.* **1992**, *27*, 1546–1552. [[CrossRef](#)]
39. Prikhod'ko, R.V.; Sychev, M.V.; Astrelin, I.M.; Erdmann, K.; Mangel, A.; Van Santen, R.A. Synthesis and structural transformations of hydrotalcite-like materials Mg₃Al and Zn₃Al. *Russ. J. Appl. Chem.* **2001**, *74*, 1573–1577.
40. Visa, A.; Maranescu, B.; Lupa, L.; Crisan, L.; Borota, A. New Efficient Adsorbent Materials in the Removal Process of Cd(II) from Aqueous Solutions. *Nanomaterials* **2020**, *10*, 899. [[CrossRef](#)]
41. Nistor, M.A.; Muntean, S.G.; Maranescu, B.; Visa, A. Phosphonate metal-organic frameworks used as dye removal materials from wastewaters. *Appl. Organomet. Chem.* **2020**, *34*, e5939. [[CrossRef](#)]
42. Lupa, L.; Maranescu, B.; Visa, A. Equilibrium and kinetic studies of chromium ions adsorption on Co(II) based phosphonate metal organic frameworks. *Sep. Sci. Technol.* **2018**, *53*, 1017–1026. [[CrossRef](#)]
43. Anitha, T.; Senthil Kumar, P.; Kumar Sathish, K.; Sriram, K.; Feroze Ahmed, J. Biosorption of lead(II) ions onto nano-sized chitosan particle blended polyvinyl alcohol (PVA): Adsorption isotherms, kinetics and equilibrium studies. *Desalin. Water Treat.* **2016**, *57*, 13711–13721. [[CrossRef](#)]
44. Mildan, E.; Gülfen, M. Equilibrium, kinetics, and thermodynamics of Pd(II) adsorption onto poly(m-aminobenzoic acid) chelating polymer. *J. Appl. Polym. Sci.* **2015**, *132*, 42533. [[CrossRef](#)]
45. Saha, P.; Chawdhury, S. *Insight into Adsorption Thermodynamics, Thermodynamics*; Mizutani, T., Ed.; IntechOpen: London, UK, 2011.
46. Sharma, S.; Rajesh, N. Augmenting the adsorption of palladium from spent catalyst using a thiazole ligand tethered on an amine functionalized polymeric resin. *Chem. Eng. J.* **2016**, *283*, 999–1008. [[CrossRef](#)]
47. Bai, F.; Ye, G.; Chen, G.; Wei, J.; Wang, J.; Chen, J. Highly selective recovery of palladium by a new silica-based adsorbent functionalized with macrocyclic ligand. *Sep. Purif. Technol.* **2013**, *106*, 38–46. [[CrossRef](#)]
48. Kumar, A.S.K.; Sharma, S.; Reddy, R.S.; Barathi, M.; Rajesh, N. Comprehending the interaction between chitosan and ionic liquid for the adsorption of palladium. *Int. J. Biol. Macromol.* **2015**, *72*, 633–639. [[CrossRef](#)] [[PubMed](#)]
49. Sharma, S.; Rajesh, N. Synergistic influence of graphene oxide and tetraoctylammonium bromide (frozen ionic liquid) for the enhanced adsorption and recovery of palladium from an industrial catalyst. *J. Environ. Chem. Eng.* **2016**, *4*, 4287–4298. [[CrossRef](#)]
50. Chen, H.; Yang, H.; Li, N.; Xue, X.; He, Z.; Zeng, Q. Palladium-Catalyzed C–N Cross-Coupling of NH-Heteroarenes and Quaternary Ammonium Salts via C–N Bond Cleavage. *Org. Process. Res. Develop.* **2019**, *23*, 1679–1685. [[CrossRef](#)]
51. Sun, J.; Li, D.; Gao, H.; Jin, Z.; Bao, M. Effect of the types of stabilizers and size distribution on catalytic activity of palladium nanoparticles in the carboxylative coupling reaction. *SN Appl. Sci.* **2019**, *1*, 137. [[CrossRef](#)]

52. Vancea, C.; Mihailescu, M.; Negrea, A.; Mosoarca, G.; Ciopec, M.; Duteanu, N.; Negrea, P.; Minzatu, V. Batch and Fixed-Bed Column Studies on Palladium Recovery from Acidic Solution by Modified MgSiO_3 . *Int. J. Environ. Res. Public Health* **2020**, *17*, 9500. [[CrossRef](#)]
53. Lupa, L.; Negrea, A.; Ciopec, M.; Negrea, P.; Raluca, V. Ionic liquids impregnated onto inorganic support used for thallium adsorption from aqueous solutions. *Sep. Purif. Technol.* **2015**, *155*, 75–82. [[CrossRef](#)]
54. Huang, Z.; Wang, C.; Zhao, J.; Wang, S.; Zhou, Y.; Zhang, L. Adsorption behavior of Pd(II) ions from aqueous solution onto pyromellitic acid modified-UiO-66- NH_2 . *Arab. J. Chem.* **2020**, *13*, 7007–7019. [[CrossRef](#)]
55. Ma, H.; Liao, X.; Liu, X.; Shi, B. Recovery of platinum(IV) and palladium(II) by bayberry tannin immobilized collagen fiber membrane from water solution. *J. Membr. Sci.* **2006**, *278*, 373–380. [[CrossRef](#)]
56. Godlewska-Żyłkiewicz, B.; Sawicka, S.; Karpińska, J. Removal of Platinum and Palladium from Wastewater by Means of Biosorption on *Fungi aspergillus* sp. and *Yeast saccharomyces* sp. *Water* **2019**, *11*, 1522. [[CrossRef](#)]